J Ther Eng, Vol. 9, No. 3, pp. 764−775, May, 2023

Journal of Thermal Engineering
Web page info: https://jten.yildiz.edu.tr
DOI: 10.18186/thermal.1300538

Journal of Thermal Engineering

Research Article

Parametric analysis of solar-assisted trigeneration system based on energy and exergy analyses

Wasim AKRAM[1], Mohd PARVEZ[2,*], Osama KHAN[3]

[1]*Department of Mechanical Engineering, Mewat Engineering College, Palla, District Nuh, Mewat, Haryana, 122107, India*
[2]*Department of Mechanical Engineering, Al-Falah University, Faridabad, Haryana, 121004, India*
[3]*Department of Mechanical Engineering, Jamia Millia Islamia University, New Delhi, 110025, India*

ARTICLE INFO

Article history
Received: 24 November 2021
Revised: 21 April 2022
Accepted: 21 May 2022

Keywords:
Rankine Cycle; Energy Efficiency; Exergy Efficiency; Molten Salt; Direct Normal Irradiance

ABSTRACT

Rapid deterioration of environment has led researchers to explore feasible forms of energy which could produce multiple energy forms with minimum inputs. Hence, in this study a novel trigeneration setup is explored so as to achieve simultaneous forms of energy in the form of electrical energy, heating and cooling, driving its primary energy requirements through a solar power tower. Molten salt is used in this study to transfer the heat from the solar component to the vapor absorption apparatus. Further the vapor absorption system is tested for thermodynamic performance for a couple of refrigerants ($LiNO_3$-H_2O and LiBr-H_2O), so as to establish the Pareto-optimal fluid among them. In order to remove any adherent error in the measuring procedure, all equipment's uncertainty analysis was performed which was negligibly small approximately at 5.34 % in terms of power plant efficiencies. An exact analysis was performed so as to estimate energy and exergy in efficiencies in the equipment while varying input parameters. Zenith exergy destruction was achieved in 33.6% by the central receiver, followed by 24.9% by heliostat, and 7.8% in heat recovery steam generator. The highest energy and exergy efficiencies (62.6% and 20.6%) are attained on system working on LiBr-H_2O, whereas (60.9% and 19.6%) were obtained in $LiNO_3$-H_2O operated system.

Cite this article as: Akram W, Parvez M, Khan O. Parametric analysis of solar-assisted trigeneration system based on energy and exergy analyses. J Ther Eng 2023;9(3):764−775.

INTRODUCTION

The last three decades or so have seen gradual growth in the applications of renewable energy for various domains probably due to extensive research and development have led to cost-effective and efficient solutions. Complications such as air pollution, fuel cost and market competitiveness associated with conventional fossil fuels have further weakened their case. Furthermore, increase in population has further depleted the existing reserves of conventional energy, since a surge has been noted as the overall electrical needs on the entire planet [1].

Among many technologies, solar thermal systems have gained considerable appreciation presumably due to the wide range of applications associated with them. This

***Corresponding author.**
*E-mail address: mparvezalig@rediffmail.com

This paper was recommended for publication in revised form by Regional Editor Ahmet Selim Dalkılıç

Published by Yıldız Technical University Press, İstanbul, Turkey

has prompted researchers to develop and examine various parameters responsible for enhancing the overall output of the system, thereby furnishing an alternative to conventional energies. Such systems provide better output when tested at the hottest time of the year [2, 3].

The conversion of solar energy into thermal energy is primarily furnished by employing special types of solar collectors such as a flat plate, evacuated tube, parabolic trough, and solar power tower plants [4-6]. Among all these solar thermal technologies, solar power tower plants (Heliostat field) technology is quite popular and has been receiving considerable attention due to its sustainable merits of producing power [7]. The thermal heat energy absorbed during the radiation process by the central receiver is further transferred to a circulating fluid usually air, water, Duratherm oil 600, or molten salt, flowing through the collector to the heat recovery steam generator (HRSG) has been established as a potential renewable refrigerant to generate steam in power plants comprehensively [8].

In recent years, several types of research have been carried out to estimate the performance evaluation of the solar-operated cogeneration and trigeneration system from energy and exergy point of view [9, 10].

The concept of exergy analysis is broadly based on the "second law of thermodynamics" which is seen as an essential tool to contemplate, identify the magnitudes, and locates the thermodynamic losses thereby pinpointing the locations of imperfection within the system. Exergy analysis shows a user-friendly way to quantify the loss of efficiency in any setup or model which consists of several types of equipment. This loss analysis helps the energy auditors to contemplate the loss summary in the energy quality. In this context, numerous studies have been reported for exergy-based analysis which is applied multiple times to compute and evaluate the exergetic analysis for solar thermal power systems [11, 12].

The application of solar thermal energy for power generation is perceived to impracticable since it has a tendency of obtaining low electric efficiency at substantially higher cost per MW [13]. However, in search of continuous pursuit of enhancement, the solar thermal power can be modified to obtain higher efficiency with lower emissions with the aid of solar energy inbuilt-based power plant. In recent times waste heat is often released into the environment without complete utilization of it, thereby resulting in substantial damages to the current environment strategies specified by governments of various countries. To utilize this waste heat based on their potential and thereby alleviating environmental problems, cogeneration, and trigeneration power cycles for solar power generation are receiving considerable attention from researchers of various renewable energy backgrounds [14, 15]. Among many popular applications, combined power, heating and cooling cycles, is the vapor absorption refrigeration cycle which is integrated at the exit of the heat user. This cycle utilizes working fluids such as $LiNO_3$-H_2O and LiBr-H_2O, which have zero ozone depletion potential using solar energy as primary input [16, 17]. Therefore, a system that produces combined electrical power, process heat, and cooling simultaneously from a single source of energy supply is known as trigeneration system and has drawn the keen interest of many researchers worldwide. There are several advantages associated with the application of trigeneration systems such as reduced greenhouse gas and emissions, lower cost of fuel, and lower electricity usage during peak winter or summer demand [18, 19].

Wang et al. [20] investigated an integrated trigeneration model whose input energy requirements were fulfilled by a flat plate collector. In this study, an optimization tool was employed for parametric evaluation and the power, cooling, and heating productions which were found approximately 6.4 kW, 5.5 kW, and 8.9 kW respectively. Eisavi et al. [21] presented the performance of novel solar-operated combined power, heating, and refrigeration system. In their results, they mentioned that the same amount of heat input, a double effect absorption refrigeration system was used instead of a single effect absorption chiller and obtained a cooling power efficiency of 48.5% and consequently it can also improve the performance of the system. Bamisile et al. [22] investigated a novel renewable energy source of trigeneration system for the simultaneous production of electricity, hot water, and cooling by employing two basic steam cycles, a gas cycle, a hot water chamber, and an absorption cycle. The complete analysis predicted the trigeneration energy and exergy efficiency for the system found to be 64% and 34.51%.

Recently, Dhahad et al. [23] explained that a progressive sustainable era can only be created if proper energy utilization of renewable sources is performed instead of using non-renewable sources. Their results indicated clearly that the system was useful for cooling instead of power generation. They also observed that the energy and exergy efficiencies of the system and the net power of the combined cycle obtained about 41.33%, 27.47%, and 158.3 kW respectively.

Rashidi et al. [24] explained the importance of integrating results of power plant components with ANN and GA. Habibi et al. [25] investigated a supercritical Brayton cycle combined with the organic Rankine cycle at bottoming that was driven by a molten salt of a solar power tower by using different working fluids for energy and exergy analysis of regenerative cycle. Their results indicated that using an organic Rankine cycle causes all three output parameters to be improved.

The primary objectives of the study are explained by four major objectives:

- To develop a solar power tower plant, which employs the heliostat field and central receiver as the concentrator receiver system so as to contemplate the repercussions of the model.
- To combine a hybrid power-solar system as a major power supplier for the model setup.

- To evaluate the thermodynamic analysis of the novel setup and further contemplate the total energy and exergy efficiencies of the various sub-systems present in the setup.
- To conduct parametric studies by considering various operating parameters and their effect on the energy and exergy efficiencies of the system.
- Evaluation of various uncertainties for each component by application of error analysis and its role in the final result.
- To study the comparative analysis between two sets of refrigerants $LiNO_3$-H_2O and LiBr-H_2O in the model setup and further estimate the best possible refrigerant among them.
- To study the role of various parameters such as direct normal irradiance (DNI), turbine inlet temperature, turbine inlet pressure, pump inlet temperature, turbine backpressure, COP on generator temperature, and irreversibility in the system on the performance of the model setup.

The properties of solar operated trigeneration system are displayed in Table 1.

SYSTEM DESCRIPTION OF SOLAR OPERATED TRIGENERATION SYSTEM

The proposed system is a solar-operated trigeneration system as depicted in Figure 1 developed by the Energy Equation Solver (EES) software. The molten salt flows through the pipes which transfer the thermal energy from the central receiver to the heat recovery steam generator (HRSG) at state point 1. The superheated steam generated in the HRSG enters the turbine at state 4 where it is expanded to produce mechanical power which is converted into electrical power by the generator coupled to the steam turbine. The reheated steam after the partial expansion is beaded and the intermediate stage for producing the process heat in the heater user at state 5 to complete the Rankine cycle. The exhaust energy transferred from the user heater proceeds to the generator of the vapor-based absorption cycle at state 6. The generator is usually employed to separate the refrigerant (often water) from the mixture of $LiNO_3$-H_2O and LiBr-H_2O with the help of steam heat. The temperature attained by the solution from heat gain predicts the overall circulation ratio of the system. As the separated refrigerant attains its required temperature usually above 90°C, it

Table 1. Properties of a solar operated trigeneration system

System properties values		
Heliostat Field	Beam radiation (DNI)	800 W/m^2
	Overall field efficiency	75%
	Total heliostat aperture area	10000 m^2
Centre Receiver	Aperture area	12.5 m^2
	The internal temperature of molten salt	290°C
	The outlet temperature of molten salt	565°C
	Tube diameter	0.019 m
	Tube thickness	0.00165 m
	Emissivity	0.8
	Reflectivity	0.04
Heat Recovery Steam Generator	The internal temperature of the water	239°C
	The outlet temperature of the steam	552°C
	Ambient temperature	25°C
Absorption Refrigeration	Generator inlet temperature	90°C
	Mixtures used in ARS	LiBr-H_2O and $LiNO_3$-H_2O
	Solubility in the waterof LiBr-H_2O	266 g/100 mL (100°C)
	Solubility in the waterof $LiNO_3$-H_2O	234 g/100 mL (100°C)
	The boiling point of LiBr-H_2O	1265°C
	The boiling point of LiBr-H_2O	600°C
Thermo – Physical Properties of Molten Salt	Temperature range	220 to 600°C
	Viscosity	25 (mPa-s)
	Density	863 (kg/m^3)
	Freezing temperature	238°C
	Melting point	221°C

further proceeds to the condenser of the system positioned as 9. Thereby it glides into the evaporator positioned at 11 which is subsequently boiled at a predefined temperature. The refrigerant leaves the evaporator at a saturated-based point at 12. This saturated state refrigerant then proceeds into the absorber, where it amalgamates with the previous weak solution at point 18 as shown in Figure 1. Due to the above operation, superheated heat is generated thereby enhancing the overall mixing efficiency of the system. The strong solution is pumped at high pressure position (SHE) at state 14 which results in the previous mixing attained within the system. This solution is further heated at the desired much higher temperature by utilizing a counter pass heat exchanger resulting in a subsequent weak solution positioned at 16. Furthermore, the cooled weak solution is expanded that eventually leads low pressure based weak solution by the application of throttling device, often throttling to be positioned at 18 back to the absorber. Primary assumption of the study is that a simulated based power plant cycle is made by combining several equipments in EES design software. Henceforth, the cycle is completed, if all the above connections remain intact.

Analysis

The following assumptions were assumed in a cycle for exergy analysis:

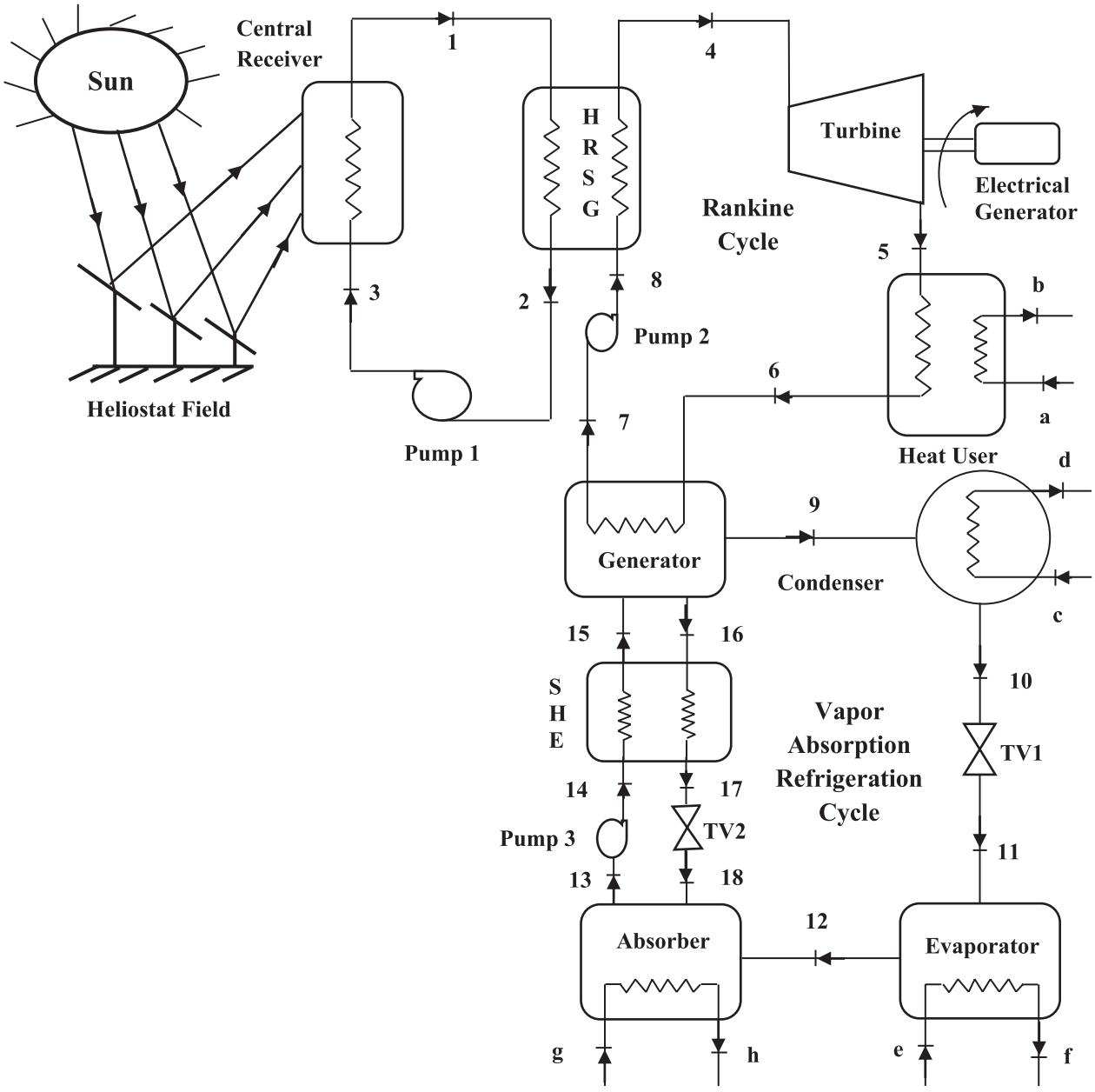

Figure 1. Solar powered trigeneration system.

- The model setups energy and exergy-based evaluation was performed during the charging phase (morning to afternoon) and discharging phase (evening tonight) for winter and summer seasons on a separate basis.
- The complete setup is assumed to work on a steady state with complete solar insulation.
- The atmospheric temperature and pressure T_0 and P_0 are assumed to be 20°C and 1.01325 bar, respectively.
- The pressure drop and ambient heat loss within various components of the setup were assumed to be insignificant and hence not taken in the overall analysis.
- Any subsequent changes in kinetic and potential energies within the setup were not taken into consideration.
- Any chemical exergy within the fuel application is neglected.
- Power consumption by the heat transfer fluid-based-pump is not considered in the analysis.

Error Estimation

The total percentage of uncertainty is determined in this study by applying the Holemans principle which is an exceptional tool in the estimation of any inherent device error present as evident from previous research [26]. Table 2 displays the errors that might be encountered while measuring various parameters in the proposed cycle.

The total percentage of uncertainty is determined in this analytical by applying the Holeman equation provided below [26]:

The total percentage uncertainty = square root of [(uncertainty in T-type thermocouples)^2 + (uncertainty in flow meter)^2 + (uncertainty in pressure transducer)^2 + (uncertainty in voltage measurement)^2 + (uncertainty in current measurement)^2 + (uncertainty in SIS sensor)^2 + (Uncertainty in power temperaturecoefficient)^2]

The total percentage uncertainty = Square root of [$(0.5)^2$ + $(0.005)^2$ + $(1.8)^2$ + $(0.06)^2$ + $(0.15)^2$ + $(5)^2$ + $(0.29)^2$]

The total percentage uncertainty = ± 5.34 %

MATHEMATICAL MODELING

The mathematical model primarily includes a thermodynamic-based analysis of the solar-operated trigeneration system which is essentially performed by employing the basic concept of a cascade. This concept aids in the evaluation of the energy and exergy methods where mass, energy, and exergy balances are written for each component. These equations later aid in searching for the exact location in the cycle whereas local irreversibilities are the highest, thereby pinpointing the main source of thermodynamic inefficiencies in the entire system.

For Heliostat

The primary function of the several stacked up heliostat field is to direct and further concentrate any incoming photonic radiations (reflects direct solar irradiations) onto the central receiver that can be expressed as:

$$\dot{Q}_{solar} = A_{field} q \tag{1}$$

where q is the number of solar radiations per unit area which may also be called direct normal irradiations (DNI) and A_{field} is specified as the area of heliostat field which is related to the aperture area (A_{pp}) in terms of concentration ratio expressed as:

$$C = \frac{A_{field}}{A_{app}} \tag{2}$$

Often the substantial amount of solar energy is efficiently utilized by the solar apparatus but some amount may be inherently lost within the environment, thereby as presented in the given equation:

$$\dot{Q}_{solar} = \dot{Q}_{CR} + \dot{Q}_{lost,heliostat} \tag{3}$$

The energy efficiency of heliostat may be defined as:

$$\eta_{energy,heliostat} = \frac{\dot{Q}_{CR}}{\dot{Q}_{solar}} \tag{4}$$

For Central Receiver (CR)

Apart from thermal energy received by the central receiver is absorbed by molten salt and the remaining is

Table 2. The measurement accuracies and analytical uncertainties associated with sensors and parameters

Sensors and parameters	Accuracies and uncertainties measurement
T-type Thermocouples	±0.5 C
Flow Meter	±5 ml
Pressure Transducer	±1.8 mbar
Voltage Measurement	±0.06 V
Current Measurement	±0.15 A
Silicon Irradiance Sensor (SIS sensor)	±5 W/m^2 ± 3.5% of measurement value
Power Temperature Coefficient	-0.29%/C

dispersed into the atmosphere as predicted from the equation specified below:

$$\dot{Q}_{CR} = \dot{Q}_{salt} + \dot{Q}_{lost,CR} = \dot{m}_{salt}(h_1 - h_3) + \dot{Q}_{lost,CR} \quad (5)$$

$$\eta_{energy,CR} = \frac{\dot{Q}_{salt}}{\dot{Q}_{CR}} \quad (6)$$

where $\dot{Q}_p$ is known as the rate of heat supplied from the plant for space heating and $\dot{Q}_E$ is energy cooling.

The net electrical power obtained from the cycle is expressed below while taking the efficiency of generation into considered:

$$\dot{W}_{el} = \eta_{gen}\dot{W}_{net} \quad (7)$$

where η_{gen} is the electrical generation efficiency.

The trigeneration based plant employed to procure power and thermal energy simultaneously, the energy-based efficiency can be stipulated to be a ratio of work obtained to the initial energy input in the system:

$$\eta_{energy,CR} = \frac{\dot{Q}_{salt}}{\dot{Q}_{CR}} \quad (8)$$

where $\dot{Q}_p$ is known as the rate of heat supplied from the plant fo space heating and $\dot{Q}_E$ is energy cooling.

The trigeneration exergy efficiency may be calculated as:

$$\eta_{en,trigen} = \frac{\dot{W}_T + \dot{Q}_E + \dot{Q}_P}{\dot{Q}_{in}} \quad (9)$$

where $\dot{E}_P = \dot{m}(h_5 - h_6) - T_0(s_5 - s_6)$ and

$\dot{E}_E = \dot{Q}_E \times \left(\frac{T_e}{T_0} - 1\right)$

where $\dot{E}_E$ is exergy cooling, and T_e is evaporative cooling temperature

The energy and exergy balance equations of each component for the solar-operated trigeneration system are given in Table 3 and Table 4.

RESULTS AND DISCUSSION

The Proposed Trigeneration System

The present research is implemented to ascertain the effects of various influencing parameters like; DNI for different working fluids employed in vapor absorption refrigeration systems (VARs), turbine inlet temperature, turbine inlet pressure, pump inlet temperature (P_2),

Table 3. Energy balance equation of each component for the solar-powered trigeneration system

Component	Energy balance equations
Trigeneration system	
Central Receiver	$\dot{Q}_{CR} = \dot{Q}_{salt} + \dot{Q}_{lost,CR} = \dot{m}_{salt}(h_1 - h_3) + \dot{Q}_{lost,CR}$
HRSG	$\dot{m}_{molt.salt}(h_1 - h_2) = \dot{m}_{ST}(h_4 - h_8)$
Steam Turbine	$\dot{W}_T = \dot{m}_{ST}(h_4 - h_5)$
Heat User	$\dot{m}_{ST}(h_5 - h_6) = \dot{m}_{hw}(h_b - h_a)$
Pump1	$\dot{W}_{P1} + \dot{m}_2 h_2 = \dot{m}_3 h_3$
Pump2	$\dot{W}_{P2} + \dot{m}_7 h_7 = \dot{m}_8 h_8$
Generator	$\dot{m}_{ST}h_6 + \dot{m}_s h_{15} = \dot{m}_r h_9 + (\dot{m}_s - \dot{m}_r)h_{16} + \dot{m}_{ST}h_7$
Condenser	$\dot{Q}_c = \dot{m}_r(h_9 - h_{10}) = \dot{m}_{cw} \times c_p(T_d - T_c)$
Expansion Valve1	$\dot{m}_{10}h_{10} = \dot{m}_{11}h_{11}$
Evaporator	$\dot{Q}_e = \dot{m}_r(h_{12} - h_{11})$
Absorber	$\dot{Q}_A = \dot{m}_r h_{12} + (\dot{m}_s - \dot{m}_r)h_{18} - \dot{m}_s h_{13}$
Pump3	$\dot{W}_{P3} + \dot{m}_{13}h_{13} = \dot{m}_{14}h_{14}$
Expansion Valve 2	$\dot{m}_{17}h_{17} = \dot{m}_{18}h_{18}$
Heat Exchanger	$\dot{Q}_{SHE} = (\dot{m}_s - \dot{m}_r)(h_{16} - h_{17}) = \dot{m}_s(h_{15} - h_{14})$

Table 4. Exergy balance equation of each component for the solar-powered trigeneration system

Component	Exergy Balance Equations
Trigeneration system	
HRSG	$\dot{E}_{D,HRSG} = T_0[\dot{m}_{salt}(s_2 - s_1) + \dot{m}_{st}(s_4 - s_8)]$
Steam Turbine	$\dot{E}_{D,T} = T_0\,\dot{m}_{st}(s_5 - s_4)$
Heat User	$\dot{E}_{D,H} = T_0[\dot{m}_{st}(s_6 - s_5) + \dot{m}_{cw}(s_b - s_a)]$
Pump1	$\dot{E}_{D,P1} = T_0\dot{m}_{salt}(s_3 - s_2)$
Pump2	$\dot{E}_{D,P2} = T_0\dot{m}_{st}(s_8 - s_7)$
Generator	$\dot{E}_{D,G} = T_0[\dot{m}_r s_9 + (\dot{m}_s - \dot{m}_r)s_{16} - \dot{m}_s s_{15} - \dot{m}_{ST}(s_6 - s_7)]$
Condenser	$\dot{E}_{D,c} = \dot{m}_r[(h_9 - h_{10}) - T_0(s_9 - s_{10})]$
Expansion Valve1	$\dot{E}_{D,EV1} = T_0\dot{m}_r(s_{11} - s_{10})$
Evaporator	$\dot{E}_{D,E} = \dot{m}_r[(h_{11} - h_{12}) - T_0(s_{11} - s_{12})]$
Absorber	$\dot{Q}_A = \dot{m}_r h_{12} + (\dot{m}_s - \dot{m}_r)h_{18} - \dot{m}_s(h_{13})$
Pump3	$\dot{E}_{D,P3} = T_0\dot{m}_s(s_{14} - s_{13})$
Expansion Valve2	$\dot{E}_{D,EV2} = T_0(\dot{m}_s - \dot{m}_r)(s_{18} - s_{17})$
Heat Exchanger	$\dot{E}_{D,SHE} = T_0[\dot{m}_s(s_{15} - s_{14}) - (\dot{m}_s - \dot{m}_r)(s_{16} - s_{17})]$

turbine backpressure on the energy and exergy efficiencies. Furthermore, the analysis also involves estimates of the irreversibility of individual components of the cycle that leads to possible implementations applied in performance enhancement of solar-operated trigeneration systems.

The gradual increments in DNI the energy and exergy efficiencies of two different working fluids ($LiNO_3$-H_2O and LiBr-H_2O) of the trigeneration system are displayed in Figure 2. and Figure 3. A marginal gain in both the efficiencies of the system was observed after a considerable increase in the DNI was provided between 600 W/m^2 to 1000 W/m^2 for both the working fluids. The foremost reason furnished for this trend is that a DNI is related to the surface temperature of a receiver and a larger increase in DNI, results in the marginal increase of receiver surface temperature. Therefore, both energy and exergy efficiencies of the proposed trigeneration system are marginally increased when the DNI increases largely. From the computed results it is further observed that the exergy efficiency of a trigeneration system is much lesser than the energy efficiency. This

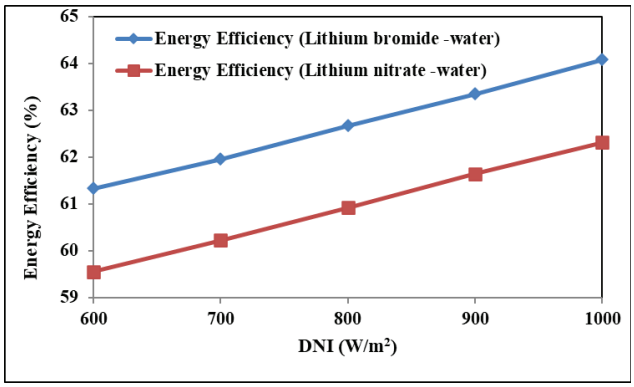

Figure 2. Variation of energy efficiency for different working fluids on DNI of a trigeneration system.

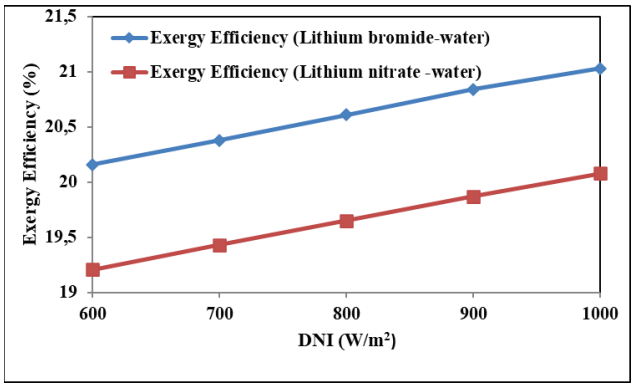

Figure 3. Variation of exergy efficiency for different working fluids on DNI of a trigeneration system.

is because the amount of exergy associated with the thermal energy of the receiver is less than its energy content; therefore, an increase in the exergy efficiency of the integrated system is much smaller than the increase in its energy efficiency. It is further perceived that both the efficiencies of LiBr-H_2O are marginally more than the $LiNO_3$-H_2O solution since inherently the absorption heat rates of LiBr-H_2O are much more than the $LiNO_3$-H_2O respectively [27].

Figure 4 shows that the variation of turbine inlet temperature on energy and exergy efficiencies observed that as an increase in turbine inlet temperature occurs, a subsequent rise in energy and exergy efficiencies of the overall trigeneration system occurred. The reason for the increase in the trend of both the efficiencies is that an evident rise in turbine inlet temperature interprets that while increasing the temperature both the heat input and power output would simultaneously increase. Besides, according to Figure 4, the exergy efficiency is less as compared to energy efficiency as a result of a rise in turbine inlet temperature [13].

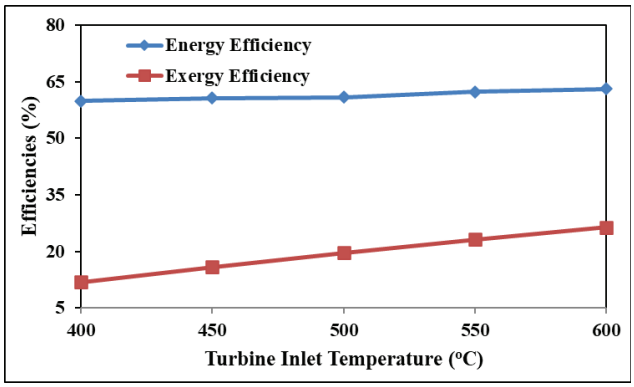

Figure 4. Variation of energy and exergy efficiencies on the turbine inlet temperature of a trigeneration system.

Figure 5 shows the effect of variation of turbine inlet pressure on energy and exergy efficiencies of the proposed trigeneration system for simultaneous production of power, heating, and cooling. It is observed that the energy efficiency is increased notably with a subsequent increase in turbine inlet pressure, whereas the exergy efficiency of a cycle decreases slightly with the same pressure. The primary reason for increasing can be attributed as the turbine inlet pressure causes an increase in refrigeration output of the absorption refrigeration and a reduction in refrigeration output of the proposed cycle as a result, the overall energy efficiency of the trigeneration system increases with the increase in turbine inlet pressure. Further, exergy efficiency decreases barely as the turbine inlet pressure increases, this is because the rate of increase in exergy output of absorption refrigeration is greater than the rate of decrease in exergy output of cycle that becomes greater than the rate of increase in exergy output of absorption refrigeration caused by a reduced mass flow rate of working fluids across the turbine [28, 29].

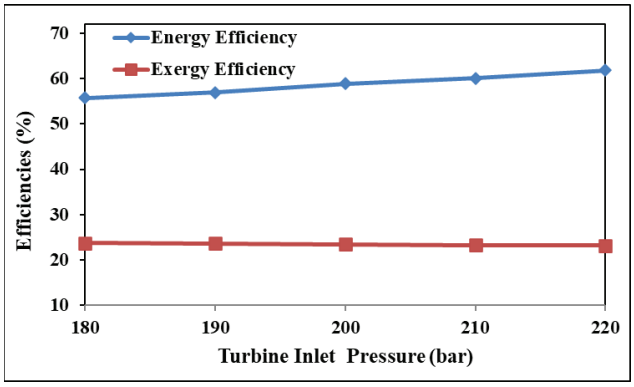

Figure 5. Variation of energy and exergy efficiencies on the turbine inlet pressure of a trigeneration system.

Figure 6 indicates the variation of the mass flow rate of molten salt and steam on DNI. It is observed that the mass flow rate of steam as well as the mass flow rate of molten salt increases as the values of DNI increase. This is due to the reason, increases in DNI causes a considerable increase in the mass flow rate of heat transfer fluid (molten salt) which in turn increases the mass flow rate of working fluid (steam) as it seen after applying the energy balance approach over the heat recovery steam generator (HRSG).

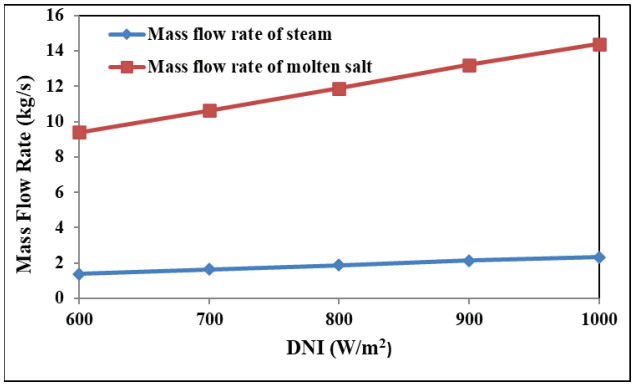

Figure 6. Variation of a mass flow rate of molten salt and steam on DNI of a trigeneration system.

Figure 7 shows the effect of pump inlet temperature (P_2) variation on the trigeneration system on energy and exergy performance considering the solar mode. It is seen that both the efficiencies were seen to increase marginally. This is due to an increase in the temperature; the overall energy

efficiency of the trigeneration system is seen to increase slightly along with increases in its exergy efficiency. It is further shown that the rise in pump inlet temperature from 90°C to 110°C compromises the energy and exergy efficiencies by less than a percent. These enhancements in energy and exergy efficiencies of the trigeneration system occur due to the reason an increase in pump inlet temperature which reduces the amount of heat required at the generator of vapor absorption refrigeration system and increased the cooling effect. This enhances the overall performance of the system.

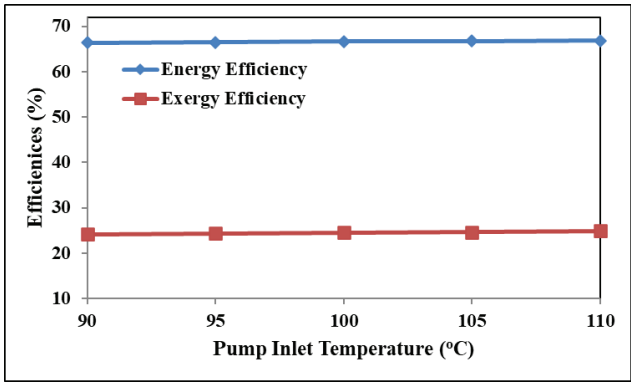

Figure 7. Variation of energy and exergy efficiencies on pump inlet temperature of a trigeneration system.

Figure 8 shows the change in turbine back pressure on the variations of energy and exergy efficiencies of a trigeneration system. It has been observed that the energy efficiency of the trigeneration cycle decreases with a subsequent increase in turbine backpressure. It was further seen that a rise in turbine back pressure from 0.06 bar to 0.14 bar causes a substantial decrease in the energy and exergy efficiencies for a trigeneration system from 34.9 % to 34.2% and 31.8% to 30.3%.

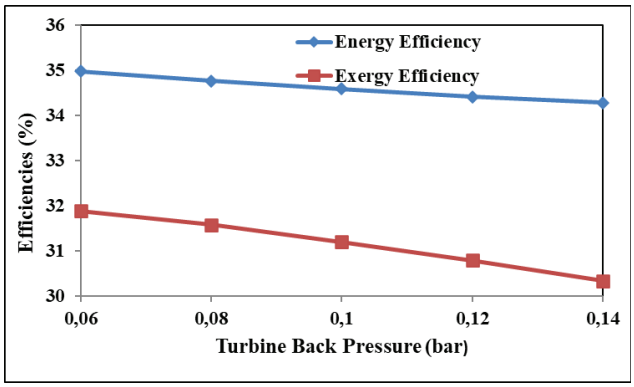

Figure 8. Variation of energy and exergy efficiencies on turbine backpressure of a trigeneration system.

Figure 9 indicated a variation in coefficient of performance (COP) with the change in generator temperature (90°C to 110°C) of vapor absorption refrigeration by using different working fluids, LiBr-H_2O, and $LiNO_3$-H_2O under the same conditions. The results indicated that the COP of LiBr-H_2O was always better and higher than the COP of $LiNO_3$-H_2O. This is because of higher solubility in water LiBr-H_2O in comparison to the $LiNO_3$-H_2O solution [28].

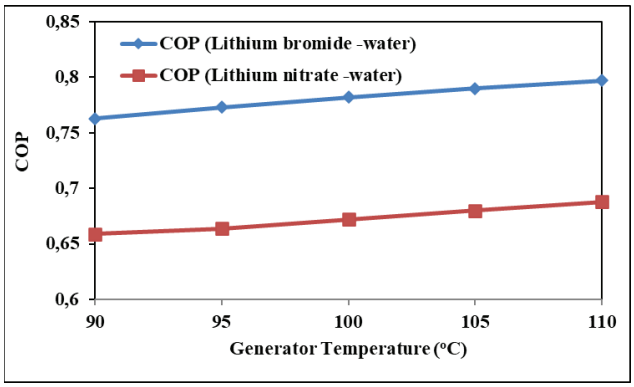

Figure 9. Variation of generator temperature on COP of a trigeneration system.

The energy and exergy output of the proposed trigeneration system combines with the change of DNI investigated and displayed in Figure 10. It has been observed that the energy output enhances considerably with a change in DNI from 600 W/m² to 1000 W/m² were increasing from 3800 kW to 6800 kW. This increasing trend is due to the reason that process heat output increases significantly as the DNI is gradually incremented over the specified range. The same increasing trends of exergy output were obtained with the change of DNI but it is much less than its corresponding energy output. This deviation is observed due to the reason the exergy accompanied by process heat and the

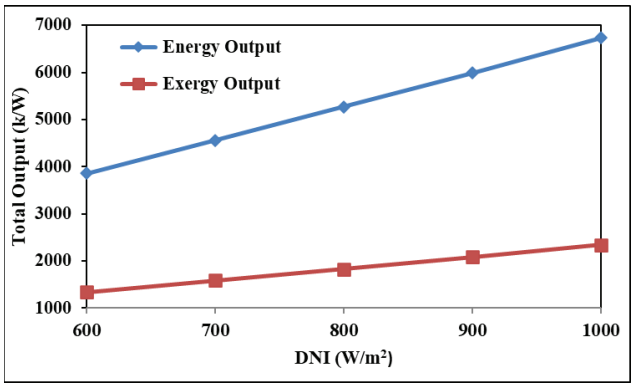

Figure 10. Variation in a change in DNI with energy and exergy output of trigeneration system.

cooling output is significantly less than their corresponding energy output since the magnitude of electrical power which gives 100% of exergy is increasing at a lower rate than the increase of their exergy associated with process heat and cooling, therefore the overall exergy output is increasing but its magnitude at all values of DNI is significantly less than the overall exergy cycle of output.

Figure 11 presents the percentage of exergy destruction in each component to find out the system feasible. In the proposed trigeneration system out of 100% exergy of the cycle, a sum of 23.9% was produced as exergetic output consisting of 16.96% turbine power, and 6.94% accompanied by process heat. It is further observed that the highest exergy destruction occurs in a central receiver which is around 33.6%. The next largest exergy destruction was observed in components such as heliostat (24.9%), HRSG (7.8%), user heat (7.2 %), and turbine (1.2%). Less than 1% of exergy destructions were observed in the rest of the components of the cycle. The overall plant generation capacity was evaluated at various DNI as displayed in the Table below. Table 5 shows the temperature and pressure at various state points.

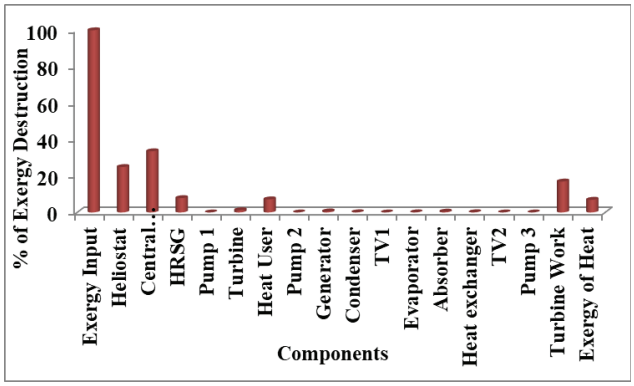

Figure 11. Exergy destruction in each component in trigeneration system.

CONCLUSIONS

The steam turbine-based trigeneration system running on solar thermal energy furnishes an exceptional model for sustainable energy transformation. This is possible through the efficient and eco-friendly utilization of abundantly available solar energy into multiple outputs of energy like power, heating, and cooling. An instrument-based error analysis predicted an error percentage of 5.83 % thereby providing accurate results. The enhancement in the performance of an energy conversion system has been evaluated after changing its mode from power generation to heating and cooling for the trigeneration system. Some of the important conclusions drawn from the energy and exergy point of view of the proposed trigeneration system may be summarized as below:

- A slight rise in the energy and exergy efficiencies was observed after a considerable increase in the value of DNI from 600 W/m^2 to 1000 W/m^2 for both the working fluids ($LiNO_3$-H_2O and LiBr-H_2O).

Table 5. Temperature and pressure at various state points

State point	Pressure (bar)	Temperature (°C)	Mass flow rate (kg/s)	Specific enthalpy (kJ/kg)	Specific entropy (kJ/kg K)
1	225	595	12.32	1580.42	7.80
2	178	290	12.32	627.80	6.98
3	178	290	12.32	627.80	9.98
4	50	500	1.7912	2433.7	6.977
5	3.172	135.5	1.7912	2727.18	6.977
6	3.172	135.5	1.7912	569.53	1.691
7	3.172	100	1.7912	419	1.307
8	3.172	101	1.7912	422	1.327
9	0.04823	90	0.1675	2660	7.480
10	0.04832	35	0.1675	175.8	0.599
11	0.00991	5	0.1675	175.8	0.6324
12	0.00991	5	0.1675	2510.7	9.0270
13	0.00991	35	2.011	187.98	0.23827
14	0.04832	35	2.011	187.98	0.23827
15	0.04832	70.5	2.011	168.15	0.42789
16	0.04832	90	1.8434	211.56	0.4912
17	0.04832	53.4	1.8434	150.27	0.30811
18	0.00991	53.4	1.8434	150.27	0.30811

- The efficiency of LiBr-H_2O is slightly higher than that based on the $LiNO_3$-H_2O solution respectively.
- Energy and exergy efficiencies increase observed marginally as turbine inlet temperature increases of a trigeneration system.
- A significant enhancement was observed when energy output increased from 3800 kW to 6800 kW with the change in DNI from 600 W/m^2 to 1000 W/m^2.
- Out of 100% s exergy input of the cycle, the highest exergy destruction is found to be about 33.6% by a central receiver, 24.93% by heliostat, and 7.86% by HRSG.

NOMENCLATURE

$\dot{A}_{app}$	Aperture area [m^2]
$\dot{A}_{field}$	Area of heliostat field [m^2]
C	Concentration ratio
$\dot{E}$	Exergy rate [kW]
$\dot{E}_D$	Exergy destruction [kW]
$\dot{E}_{x,in}$	Exergy input to the plant [kW]
HRSG	Heat recovery steam generator
h	Enthalpy [kJ/kg]
LiBr-H_2O	Lithium bromide-water
$LiNO_3$ - H_2O	Lithium nitrate-water
$\dot{m}$	Mass flow rate [kg/s]
$\dot{m}_{cw}$	Mass flow rate of cold water [kg/sec]
$\dot{m}_{hw}$	Mass flow rate of hot water [kg/s]
$\dot{m}_r$	Mass flow rate of refrigerant [kg/s]
$\dot{m}_s$	Mass flow rate of solution [kg/s]
$\dot{m}_{ST}$	Mass flow rate of steam [kg/s]
$\dot{m}_{salt}$	Mass flow rate of molten salt [kg/s]
q	Amount of solar radiation per unit area [W/m^2]
P	Pump
$\dot{Q}_A$	Energy of the absorber [kW]
$\dot{Q}_C$	Heat energy of condenser [kW]
$\dot{Q}_{CR}$	Heat energy of the central receiver [kW]
$\dot{Q}_E$	Energy of the evaporator [kW]
$\dot{Q}_{in}$	Heat energy rate in [kW]
$\dot{Q}_{lost,CR}$	Loss of heat energy from the central receiver [kW]
$\dot{Q}_{lost,heliostat}$	Loss of heat energy from heliostat [kW]
$\dot{Q}_P$	Process heat [kW]
$\dot{Q}_{salt}$	Heat energy of molten salt [kW]
$\dot{Q}_{solar}$	Heat energy of solar [kW]
SHE	Solution heat exchanger
s	Specific entropy [kJ/kg K]
T_0	Ambient temperature [°C]
VARs	Vapor absorption refrigeration system
$\dot{W}_{el}$	Electrical power [kW]
$\dot{W}_{net}$	Net power [kW]
$\dot{W}_P$	Pump [kW]
$\dot{W}_T$	Turbine work [kW]
$\eta_{eN,tri}$	Energy efficiency of a trigeneration system
$\eta_{ex,tri}$	Exergy efficiency of a trigeneration system
$\eta_{energy,heliostat}$	Energy efficiency of heliostat
η_{gen}	Electrical efficiency
a–h,1–18	State points of a trigeneration system

AUTHORSHIP CONTRIBUTIONS

Authors equally contributed to this work.

DATA AVAILABILITY STATEMENT

The authors confirm that the data that supports the findings of this study are available within the article. Raw data that support the finding of this study are available from the corresponding author, upon reasonable request.

CONFLICT OF INTEREST

The author declared no potential conflicts of interest with respect to the research, authorship, and/or publication of this article.

ETHICS

There are no ethical issues with the publication of this manuscript.

REFERENCES

[1] Dincer I. Renewable energy and sustainable development: a crucial review. Renew Sustain Energy Rev 2000;4:157−175. [CrossRef]

[2] Becker M, Macias M, Ajon JI. Solar thermal power stations, the future for renewable energy: Prospects and Directions. EUREC Agency. London: James & James Science Publishers; 1996. p. 135−153.

[3] Kumar CR, Majid MA. Renewable energy for sustainable development in India: current status, future prospects, challenges, employment, and investment opportunities. Energy Sustain Soc 2020;10:1−36. [CrossRef]

[4] Kalogirou SA. Solar thermal collectors and applications. Prog Energy Combust Sci 2004;30:231−295. [CrossRef]

[5] Yaglı H, Karakus C, Koc Y, Çevik M, Ugurlu I, Koc A. Designing and exergetic analysis of a solar power tower system for Iskenderun region. Int J Exergy 2019;28:96−112. [CrossRef]

[6] Moosavian SF, Borzuei D, Ahmadi A. Energy, exergy, environmental and economic analysis of the parabolic solar collector with life cycle assessment for different climate conditions. Renew Energy 2021;165:301−320. [CrossRef]

[7] Rabbani M, Ratlamwala TAH, Dincer I. Development of a new heliostat field-based integrated solar energy system for cogeneration. Arab J Sci Eng 2018;43:1267−1277. [CrossRef]

[8] Schottl P, Bern G, Rooyen DWV, Pretel JAF, Fluri T, Nitz P. Optimization of solar tower molten salt cavity receivers for maximum yield based an annual performance assessment. Sol Energy 2020;199:278−294. [CrossRef]

[9] Mohammadi K, McGowan JP. Thermodynamic analysis of hybrid cycles based on a regenerative steam Rankine cycle for cogeneration and trigeneration. Energy Convers Manag 2018;158:460−475. [CrossRef]

[10] Parvez M, Khalid F, Khan O. Thermodynamic performance assessment of solar based combined power and absorption refrigeration cycle. Int J Exergy 2020;31:232−248. [CrossRef]

[11] Bejan A. Fundamentals of exergy analysis, entropy generation minimization, and the generation of flow architecture. Int J Energy Res 2002;26:545−565. [CrossRef]

[12] Dincer I, Rosen MA. Exergy: energy, environment and sustainable development. 2nd ed. Oxford, UK: Elsevier; 2012. [CrossRef]

[13] Xu C, Wang Z, Li X, Sun F. Energy and exergy analysis of solar power tower plants. Appl Therm Eng 2011;31:3904−3913. [CrossRef]

[14] Fito J, Ramousse J, Hodencq S, Wurtz F. Energy, exergy, economic and exergoeconomic (4E) multicriteria analysis of an industrial waste heat valorization system through district heating. Sustain Energy Technol Assess 2020;42:100894. [CrossRef]

[15] Akrami E, Ameri M, Rocco MV, Sanvito FD, Colombo E. Thermodynamic and exergo-economic analyses of an innovative semi self-feeding energy system synchronized with waste-to-energy technology. Sustain Energy Technol Assess 2020;40:100759. [CrossRef]

[16] Luo C, Su Q, Mi W. Thermophysical properties and application of $LiNO_3$-H_2O working fluid. Int J Refrig 2013;6:1689−1700. [CrossRef]

[17] Kerme ED, Chafidz A, Agboola OP, Orfi J, Fakeeha AH, Al-Fatesh AS. Energetic and exergetic analysis of solar-powered lithium bromide-water absorption cooling system. J Clean Prod 2017;151:60−73. [CrossRef]

[18] Saini P, Singh J, Sarkar J. Proposal and performance comparison of various solar-driven novel combined cooling, heating and power system topologies. Energy Convers Manag 2020;205:112342. [CrossRef]

[19] Parikhani T, Azariyan H, Behrad R, Ghaebi H, Jannatkhah J. Thermodynamic and thermoeconomic analysis of a novel ammonia-water mixture combined cooling, heating, and power (CCHP) cycle. Renew Energy 2020;145:1158−1175. [CrossRef]

[20] Wang M, Wang J, Zhao P, Dai Y. Multi-objective optimization of a combined cooling, heating and power system driven by solar energy. Energy Convers Manag 2015;89:289−297. [CrossRef]

[21] Eisavi B, Khalilarya S, Chitsaz A, Rosen MA. Thermodynamic analysis of a novel combined cooling, heating and power system driven by solar energy. Appl Therm Energy 2018;129:1219−1229. [CrossRef]

[22] Bamisile O, Huang Q, Anane POK, Dagbasi M. Performance analyses of a renewable energy powered system for trigeneration. Sustainability 2019;11:1−15. [CrossRef]

[23] Dhahad HA, Hussen HM, Nguyen PT, Ghaebi H, Ashraf MA. Thermodynamic and thermoeconomic analysis of innovative integration of Kalina and absorption refrigeration cycles for simultaneously cooling and power generation. Energy Convers Manag 2020;203:112241. [CrossRef]

[24] Rashidi M. A., Bég O. A. Parsa A. B., Nazari F., 2011. Analysis and optimization of a transcritical power cycle with regenerator using artificial neural networks and genetic algorithms, Proc Inst Mech Eng Part A J Power Energy 2011;225:701−717. [CrossRef]

[25] Habibi H, Zoghi M, Chitsaz A, Javaherdeh K, Ayazpour M, Bellos E. Working fluid selection for regenerative supercritical Brayton cycle combined with bottoming ORC driven by molten salt solar power tower using energy-exergy analysis. Sustain Energy Technol Assess 2020;39:100699. [CrossRef]

[26] Holman JP. Experimental techniques. India: Tata McGraw Hill Publications; 2003.

[27] Parvez M, Khan ME, Khalid F, Khan O, Akram W. A novel energy and exergy assessments of solar operated combined power and absorption refrigeration cogeneration cycle. In: Patel N, Bhoi AK, Padmanaban S, Holm-Nielsen JB, editors. Electric vehicles, green energy and technology. 1st ed. Berlin: Springer; 2021. p. 213−229. [CrossRef]

[28] Khaliq A, Kumar R, Mokheimer EMA. Investigation on a solar thermal power and ejector-absorption refrigeration system based on first and second law analyses. Energy 2018;164:1030−1043. [CrossRef]

[29] Zheng Z, Cao J, Wu W, Leung MKH. Parallel and in-series arrangements of zeotropic dual-pressure Organic Rankine Cycle (ORC) for low-grade waste heat recovery. Energy Rep 2022;8:2630−2645. [CrossRef]